

Comparison of PCB Based Actuator Coils for Untethered Actuation

Erdem Doguş Akkuş^{1*}, Levent Çetin²

¹ Robotic Engineering, Graduate School of Natural and Applied Sciences, İzmir Kâtip Çelebi University, İzmir, Turkey

² Mechatronics Engineering Department, İzmir Kâtip Çelebi University, İzmir, Turkey

¹ e.dogus.akkus@gmail.com; ² levent.cetin@ikc.edu.tr

* Corresponding Author

ARTICLE INFO

ABSTRACT

Article history

Received February 28, 2023

Revised April 07, 2023

Accepted April 10, 2023

Keywords

Planar Coil;

Untethered Actuation;

PCB Coil;

Micromachines

Recently magnetic actuation has become a versatile tool for manipulation on both the micro and macro scales. Due to the problems arising from scale, conventional electromagnet production methods are insufficient to produce the desired electromagnets to be used for this purpose. To solve the problems arising from this situation, researchers have been forced to work in alternative electromagnet production and application areas and pave the way for PCB-based electromagnetic actuators. For this reason, this article will explain the design principles of PCB planar coils for electromagnetic actuator applications and will provide the basis for later studies to create a coil matrix using this coil design and an actuator that can move ferromagnetic particles or magnets in the plane with this 2D coil matrix. First of all, to be able to design a coil that consists of copper paths on the PCB and can meet expectations (homogeneous magnetic field, high magnetic force/current ratio). PCB coils consisting of square, circular and hexagonal coils are manufactured, and various measurements are made. The measured results are consistent with the simulated results proving the accuracy and applicability of PCB coil actuators, and they are highly suitable for a new actuator version. In the tests carried out, coils energized with 1A can provide a maximum field strength of 1400 (A/m) and an average of 900 (A/m) and due to the lack of magnetic core, the created magnetic field has the shape of a bell. In order to overcome this situation, it is foreseen that conducting studies to increase the working current and, as a more important development, switching from the planar single-layer structure to the structure of two or more layers can increase the magnetic field produced by this type of coils. But this layer increase should take into account the cost, and PCB production and application capabilities should be made available.

This is an open-access article under the [CC-BY-SA](https://creativecommons.org/licenses/by-sa/4.0/) license.



1. Introduction

For several decades, developments in technology have converted small-scale machines from science fiction elements to real-world practices. The small vessels navigating in living bodies [1, 2, 3] and fully functional nano and microscale electromechanical systems [4, 5, 6] have been reported for exploiting the technology for further use by mankind. An important requirement for proper operation of micromachines for active sensing and actuation is power transfer. Although the

embarked actuators on small scale are proposed [7, 8], it is also known that they increase dimensions of the micromachines. Hence, an accepted methodology in miniaturization of the machines is untethered power transfer.

A microscale robotic system can be defined as a set of coupled systems for wireless power transfer and untethered microscale rig. The wireless power transfer can be realized by exploiting different means of sources: ultrasound [9, 10], electric fields [11] and magnetic fields [12]. The magnetic fields are shown to be more versatile than the other actuators in terms of simplicity and efficiency of the operations [13].

The alternative sources for untethered magnetic actuation are permanent magnets and electromagnets [14]. Although they have the same means of actuation (magnetic field), they are different in terms of the applied control methodologies [15, 16, 17, 18]. The permanent magnets have large power-to-volume density, but they cannot be switched off; hence they create unwanted effects during coupling and uncoupling from the untethered microparticle. At the same time, the electromagnets are very well controlled through any segment of the operation by controlling the driving current despite the fact that they are relatively weak in terms of power density [19].

The electromagnets are coils. The magnetic field arising from the coils becomes weaker as distance to the workspace becomes longer. Two different strategies are proposed for overcoming this attenuation: increasing the field strength via core structure or designing compact coils. The choice of strategy depends on the application scenario. The PCB coils can be good alternatives for actuation requirements in case of planar manipulation [20] tasks that are carried out in limited workspace. In this context, a group of PCB coils [21] are said to be good alternatives as actuators in micromanipulation tasks, which involve mixing, separation and assembly.

The PCB coil design problem is mainly addressed in different areas of electromagnetics, like power transfer systems and antenna design. The design steps are excessively different from conventional coil design steps. Although the PCB coil design stages start with finding the target usage area, the target design criteria are determined, and then the design is made considering the production abilities. When we look at the literature, the targeted non-contact electromagnetic actuator designs are generally not PCB-based, while the PCB-based ones have made general assumptions in their coil designs and have not touched upon this issue.

Terms of PCB coil refer to a wide variety of coil types. There is no design constraint about geometry, shape or any other design parameters since PCB production uses photolithography [22, 23] to remove unwanted copper and store predicted patterns. However, the geometric shapes studied are generally round, square, and hexagonal and can be in the form gathered from these geometries, or they can be in very different shapes that do not comply with the standard coil perception [24, 25]. The coil types aimed to be investigated in this study will be oval and square hexagons, as mentioned above. The main purpose of choosing these design types is to find out whether there is a difference between coils with similar dimensions and design values but with different geometric shapes and to find the optimum geometry for magnetic actuators [26].

Although the presented papers demonstrated successful actuation results for PCB coil-based actuators, the coil geometries were not analyzed separately to optimize actuator performance. Hence, the contribution of the research is a comparison of the planar coil shapes [11] in terms of their compatibility with untethered actuation. The presented results demonstrate the force-inducing capability of proposed coil shapes. The rest of the paper is organized as follows. In the second chapter, the theoretical background for coil properties and means of comparison are given. In the third chapter, the simulation and experimental results are presented, and the theoretical results are discussed. In the last part of the paper, results and future work are mentioned.

2. Method

The suitability of a coil shape for being a compact untethered actuator can be evaluated from three different aspects, in terms of electrical characteristics, magnetic characteristics and fill ratio of the coils on PCB.

2.1. Mathematical Model of a PCB Coil

For realistic modeling, a coil can be represented as a combination of ideal components; hence its effect on circuit is not a single inductive reactance but an impedance. The model of a coil can be generalized as given in Fig. 1 (a).

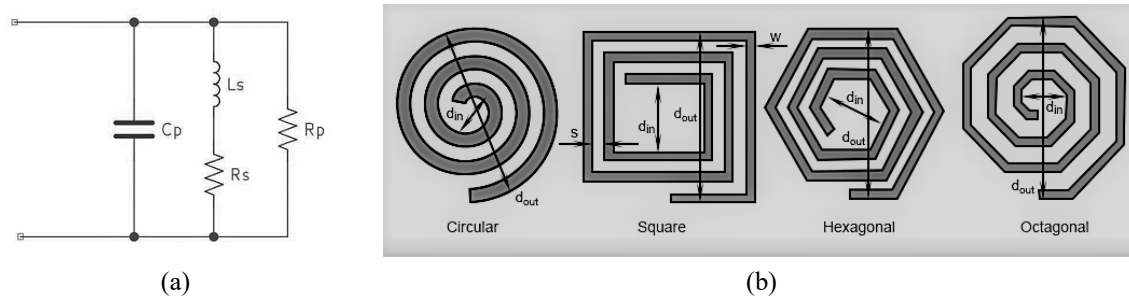


Fig. 1. Model of PCB Coil (a), Planar Coils Types (b) [12]

The coil exhibits small DC series resistance due to its specific resistivity (R). The magnetic energy dissipation due to environmental interactions is modeled by placing a resistor in parallel (R_p) with the coil inductance. The parallel capacitor (C_p) represents electrical coupling between coil loops. The mathematical model of the system can be obtained using Kirchhoff's Current Law as in Equation (1) in Laplace Domain.

$$i_0(s) = C_p s V_0(s) + \frac{V_0(s)}{R + Ls} + \frac{V_0(s)}{R_p} \quad (1)$$

For PCB coil-based setups, the energy dissipation due to magnetic losses (Eddy Current-like) is negligible similar to stored electrical energy in parallel capacitors. Concerning the given fact that the C_p has a value negligibly small whereas R_p has a very large value, Equation (1) can be simplified as (2).

$$i(s) = \frac{V_0(s)}{R + Ls} \quad (2)$$

Concerning Equation (2), two parameters can be defined: ohmic loss (P_{loss}) and quality factor (or Q) of PCB coils. For each formula of these parameters, shown in Equation (3) for P_{loss} and Equation (4) for Q . Ohmic loss term stands for power loss due to parasitic resistance of copper windings of PCB coils. Resistance of PCB traces can be calculated using Equation (5). On the other hand, quality factor term stands for ratio between resistance and inductance of PCB coil. The winding resistance appears as a resistance in series with the inductor; This is named as R_{DC} (DC resistance) or parasitic resistance. This parasitic resistance dissipates real power in the system and dampens the system. An inductor's quality factor (or Q) is the ratio of its inductive reactance to its resistance at a given frequency and is a measure of its efficiency. The higher the Q factor of the inductor, the closer it approaches the behavior of an ideal inductor. For resonant tank circuits, it is desirable to use higher Q -value inductors. For electromagnet quality factor can be related to power loss since higher Q means low series resistance, low power loss and also lower heat generation.

$$P_{loss} = R^2 i \quad (3)$$

$$Q = \frac{wL}{R} \quad (4)$$

For calculating the parameters, the series resistance of the coil is calculated concerning the PCB trace. PCB traces are created by chemically etched from plain copper. The chemical removes away the copper from top to bottom as a result of chemical process, creating a copper track that has trapezoidal shape rather than square. If the traces are bigger than 0.1mm, then the effect of nonuniform shape is negligible. Concerning resistivity is a function of not constant but varies with change in temperature; temperature (T) and the Temperature Coefficient of Resistance (α) should be taken into account. The resistance of a track can then be expressed by Equation (5).

$$R = \left(\rho \frac{L}{A}\right)(1 + \alpha(T - T_{ref})) \quad (5)$$

where T_{ref} is 20 °C, temperature coefficient of copper(α) is $4.04 \times 10^{-3} \text{K}^{-1}$ and specific resistivity of copper(ρ) at 20 °C is $1.68 \times 10^8 \Omega \cdot \text{m}$.

The Modified Wheeler Equation [13] (6) can be used to calculate the inductance of a single-layer spiral coil. Wheeler presented several formulas for planar spiral inductors, which were intended for discrete inductors that are simple types of radio-frequency coils. Respecting the originally published paper, these formulas are correct to within 5 percent for coils with $r_{avg} > 0.2 \left(\frac{d_{out} - d_{in}}{2}\right)$.

$$L = \frac{31.33\mu_0 n^2 r_{avg}^2}{8r_{avg} + 11\left(\frac{d_{out} - d_{in}}{2}\right)} \quad (6)$$

Equation (6) can be used to calculate the inductance of a single-layer circular spiral coil where L is inductance (H) and n is number of turns and r_{avg} is average radius, in meters (m), d_{out} is outer diameter of coil, d_{in} is inner diameter of coil.

For square, hexagonal, and octagonal, another format of Wheeler Equation (7) can be used as

$$L = \frac{K_1 \mu_0 n^2 d_{avg}}{1 + K_1 p} \quad (7)$$

where K_1 and K_2 are dimensionless coefficients that can be found in Table 1, p can be calculated as (8).

$$p = \frac{d_{in} - d_{out}}{d_{in} + d_{out}} \quad (8)$$

Table 1. Modified Wheeler formula coefficients

Coil Types	Coefficients	
	K_1	K_2
Square	2.34	2.75
Hexagonal	2.33	3.82
Octagonal	2.25	3.55

IPC-2221 Generic Standard on Printed Board Design [30] is an accepted industry standard that defines a multitude of PCB design aspects. The requirements in the standard define certain design constraints that are intended to ensure safety, reliability, and manufacturability. The qualifications in the standard are generic standards; more specific standards applying to different types of boards are found throughout the 2220 series of standards. Some examples include design requirements regarding materials (including substrates and coating), testability, thermal management and thermal reliefs and annular rings and so on. The IPC-2221 standard is a generic printed circuit board qualification and accepted standard for PCBs/PCBAs.

According to IPC-2221 standard general working temperatures of PCBs are between 0 to 100 C degrees and working current below so 30A. IPC-2221 provide graphs and test result at that region so that derived formulas in Equation (9) is valid between these parameters. The capability of trace to carry current is directly proportional to the cross-sectional area of trace and temperature rise. In high-current applications, PCBs have high-width copper traces. Hence it is very important for PCB layout design engineers to know what trace width should be selected for a particular power circuit or device. This would increase the current carrying capacity and durability of the PCB coil, as for the supporting coefficients on IPC-2221, which are shown in Table 2.

Table 2. IPC-2221 pre-calculated coefficients

Layers	Coefficients		
	k	b	c
Internal layers	0.024	0.44	0.725
External layers	0.048	0.44	0.725

$$A = \left(\frac{I}{kT_{rise}^b} \right) \left(\frac{1}{c} \right) \quad (9)$$

In Equation (9), A is the cross-sectional area of PCB trace, k , b and c are IPC coefficients which are given in Table 2, T_{rise} is temperature rise of PCB. So a new equation is obtained as in (10) as

$$T_{int} = T_{rise} + T_{amb} \quad (10)$$

where T_{int} and T_{amb} are initial and ambient temperatures, respectively.

2.2. Magnetic Field

The prime interest in coils, in terms of actuation, is their capability of inducing magnetic fields in a workspace. Therefore, two aspects should be considered in comparison: magnetic field and magnetic force.

In the most general case, the magnetic field analysis is carried out by solving Maxwell equations. In the context of the paper, all of the studies are held in the stationary domain with constant current. The material of the coil trace was chosen as copper, and FR4 PCB substrate was defined around the coil. Hence, the generated magnetic field H by the PCB coil can be calculated by Ampère Law as in (11) as

$$\nabla \times H = J \quad (11)$$

where J is current density (A/m²), and it can be calculated by Ohm's Law as (12) as

$$J = \sigma E + J_e \quad (12)$$

where σ is the conductivity of the copper (inverse of specific resistivity), E is the electrical field, and J_e is the applied current density.

The given set of equations can be solved simultaneously for any defined geometry by using finite element method. When magnetic field is obtained, the magnetic force can be calculated as given in (13) [31] as

$$F = v(M \cdot \nabla)B \quad (13)$$

where F is magnetic force, v is volume, and M is magnetization of permanent magnet. The magnetic flux density (B) can be calculated with the constitutive equation $B = \mu H$ for the calculated magnetic field (H). The magnetic force calculations are carried out concerning a work plane above PCB coil and cylindrical permanent magnet (details of geometry are given in Section 3.3 in Fig. 6 and Fig. 7).

2.3. Fill Ratio of the Coils on PCB

The coils analyzed in this study were used in 2d coil matrices to create linear actuators. The important thing in this type of 2d coil matrices is the filling rate and layout. The term fill rate can be explained

as (14), which is the maximum number of coils that can be placed per unit area. The main goal is not to leave any spaces in the work area. Although it eliminates the magnetic field gaps where the magnet can fall, it does not eliminate the asymmetrical behavior in the direction of movement. In Equation (14), f is filling rate, N is number of coils, and A is working area.

$$f = \frac{N}{A} \quad (14)$$

The layout is how and how close the coils used can be placed and how easily the electrical connections can be made. Although it is thought that the placement can be done geometrically, this situation varies considerably in practice. This situation makes a difference depending on the number of layers of the PCB used, the process capabilities of the PCB manufacturer and the designer's methods. Since this problem is so deep and depends on variables, there is no specific formula or solution for this problem. It is more appropriate to leave cost or application aspects.

3. Results and Discussion

3.1. Experimental Coil Designs

Three different trial coils were designed with the above-mentioned design criteria. These are square, circular, and hexagonal coils. All three coils are designed with similar features, except for some operational design difficulties since these designs need to be producible so that calculation and simulation can be tested in the real world. Design parameters of the PCBs selected in mind today's standard manufacturing abilities. Currently, Standard PCB production specifications are as follows; minimum 0.25 mm thick tracks, 0.25 mm distance between tracks, 0.6/0.3 mm via diameter and hole diameter. Features in this style have become the production standard in the industry [27]. The coils in the continuation of the study, designed to keep the cost at a minimum, taking these features into consideration coils are designed as in Table 3. The remaining calculations, design and test, are made with respect to these parameters.

Table 3. Coil design parameters for different coil types, such as circular, square and hexagonal

Design Parameters	Coil Types		
	Circular coil	Square coil	Hexagonal coil
Number of turns	11	11	11
Track With	0.25 mm	0.25 mm	0.25 mm
Spacing	0.25 mm	0.25 mm	0.25 mm
Dout	13.250 mm	11.750 mm	11.45 mm
Din	2.75 mm	1.25 mm	2.92 mm
Total trace length	273 mm	286mm	252 mm

For tests as in Table 2 and Table 3, different planar coils were designed using kiCAD electronic design tool and manufactured in China. As shown in Fig. 2, PCBs are two layers. Coils themselves are located on top copper layer, and for electrical connection to appropriate connector bottom copper layer and through-hole vias are used so that coils have uniform shape and have no interruption. They are circular, square, and octagonal coils. For evaluation performance of different designs, conventional methods measure inductance, resistance and magnetic field. Inductance and resistance were measured with LCR meter [28, 29].

The series resistance and inductance of all coils have been calculated with the above-mentioned series resistance and inductance calculation formulas (5), (6), (7) and Table 1, Table 2, and Table 3. In order to test whether the calculated values are actually consistent or not, as shown in Table 4, PCB coils that exactly match the simulation parameters was tested. For measurements Lutron brand LCR9184 LCR meter is used. It has DC resistance of 0.015 ohms and inductance of 0.15 μ H in its test leads. Afterward, all the coils are connected to a connector with the ends of the bottom layer of copper. With these connectors, the coils were connected to the meter and examined. In order not to disturb the measurements, these paths are placed as short as possible and close to each other.

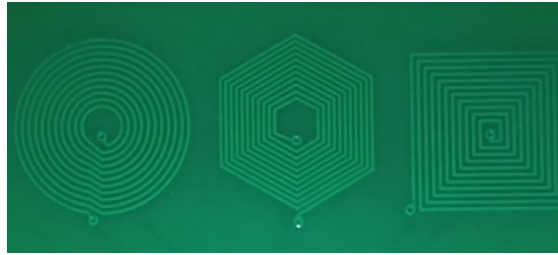


Fig 2. Printed planar coils

Table 4. Calculated and measured coil parameters for various coil types

Coil Types	Resistance		Inductance		Current Capacity
	R_{cal} (Ω)	R_{mrds} (Ω)	L_{cal} (μH)	L_{mrds} (μH)	I_{max} (A)
Circular Coil	0.588	0.70	0.849	0.896	2.65
Square Coil	0.616	0.72	0.718	0.804	2.65
Hexagonal Coil	0.542	0.70	0.778	0.915	2.65

In Table 4, R_{cal} is calculated resistance in ohms, R_{mrds} is measured resistance in ohms, L_{cal} is calculated inductance in Henries, L_{mrds} is measured inductance in Henries, I_{max} is maximum working current of the coils.

The current capacity of the coils was calculated using Equation (8) and Table 3. In fact, these calculations were taken into account while designing. The authors determined 1 A or more as operating current for coils as design parameters and also made an interpolation between considerable current amplitudes and coil sizes while determining these numbers and tried to determine the most appropriate parameters.

3.2. Magnetic Field Analysis

A good example of comparing coils is the magnetic field strength they produce, the dispersion and density of the magnetic field. In order to compare the magnetic fields produced by the coils, a series of simulations were made, and the parameter was determined as in Fig. 3, Fig. 4, and Fig. 5 for the result. The magnetic field is the norm, and the magnetic field force is on the horizontal axis. The simulation conditions are as follows; All coils are energized with 1 Ampere. Since the magnetic field will decrease as you move away from the center of the coil on the vertical axis, it is necessary to determine the approximate operating distance. This is selected as 1mm. In other words, the measurement magnetic field was determined as 1 mm above the coil on the vertical axis and ∓ 13 mm on the horizontal axis.

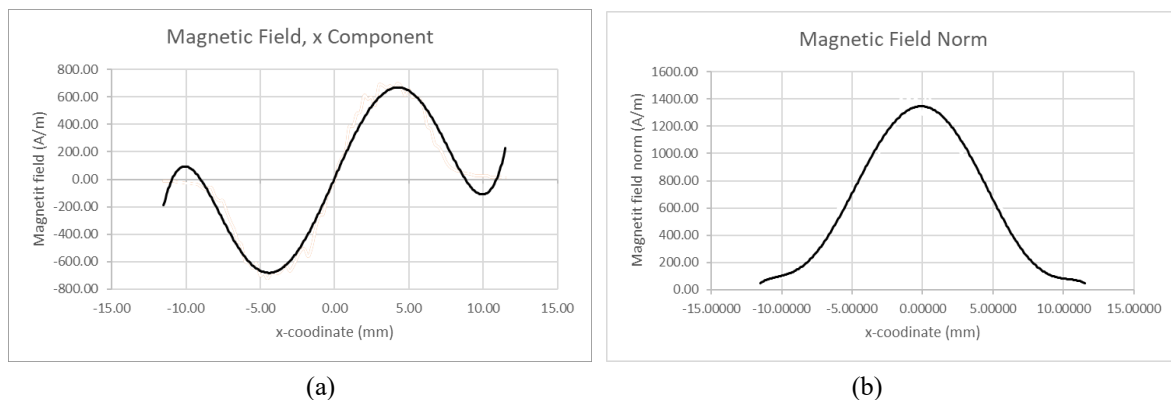


Fig. 3. Magnetic field strength in motion direction (a) and Magnetic field norm (b) of circular coil

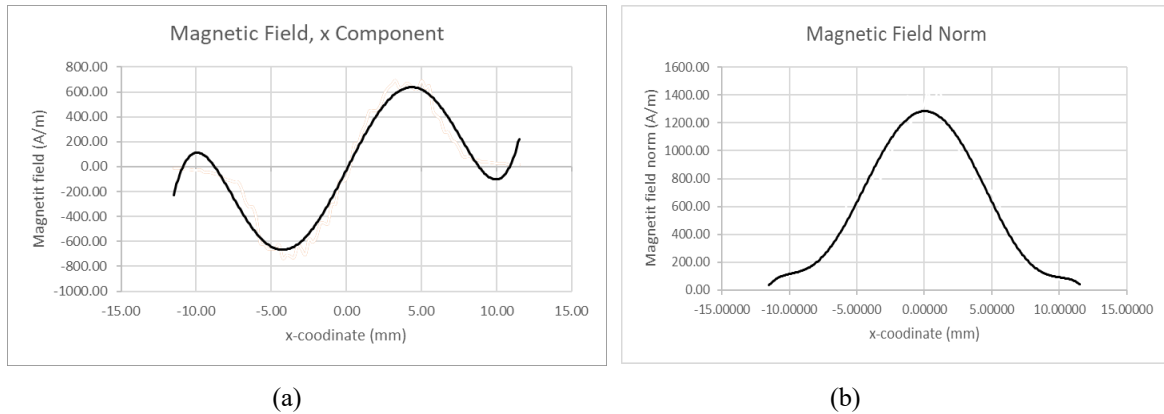


Fig. 4. Magnetic field strength (a) and Magnetic field density norm (b) of square coil

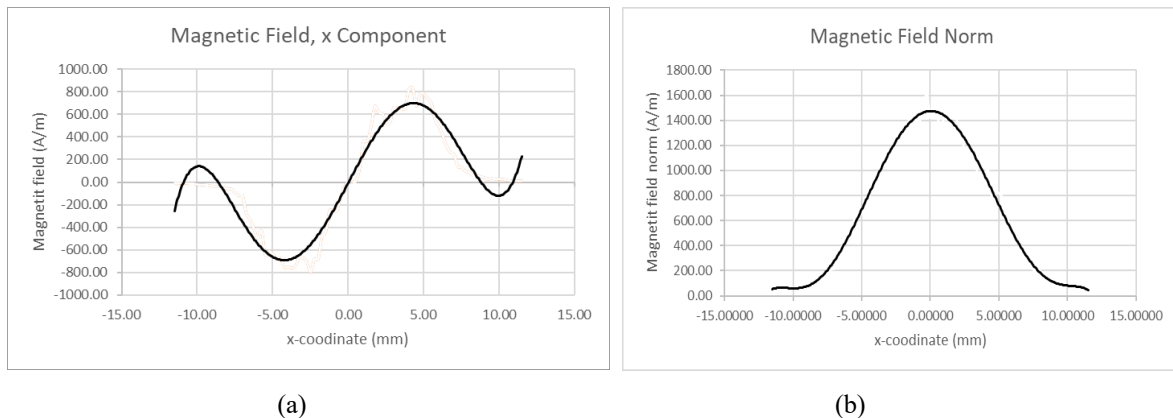


Fig. 5. Magnetic field strength (a) and Magnetic field density norm (b) of hexagonal coil

Fig. 3, Fig. 4, and Fig. 5 (a) show magnetic field strength in the x-axis of circular, square and hexagonal coils, respectively. As expected, field strength reduces to zero and changes direction at the coil center, which means horizontal force will be zero at this point. In order to look at the homogeneity of the magnetic field produced by the PCB coils, we need to look at the magnetic field norm. As seen in Fig. 3, Fig. 4, and Fig. 5 (b), the magnetic field has the shape of a bell. This is due to the fact that the coils have a coreless structure. The magnetic field increases towards the center, indicating that the magnetic force will be greater at the center than at the edges. When we examine all the graphics, we see that the coil that produces the most magnetic field strength is the hexagonal coil.

3.3. Magnetic Force

In order to see magnetic force acting on a permanent Neodymium magnet, a simulation setup has been designed, as shown in Fig. 6 and Fig. 7.

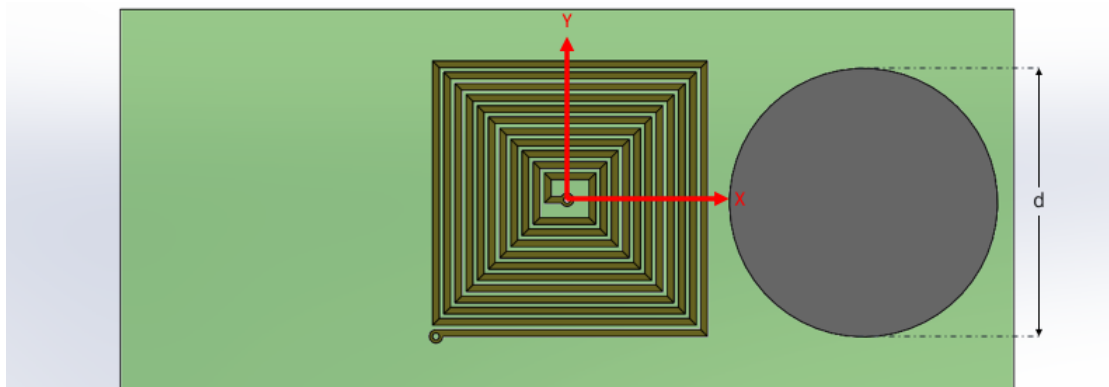


Fig. 6. Magnetic force simulation setup top view

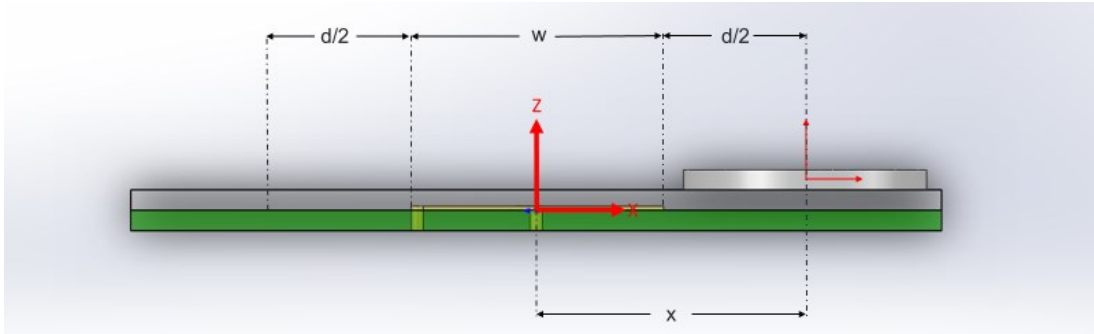


Fig. 7. Magnetic force simulation setup side view

A series of simulations were made to see the effect of the magnetic field produced by the coils on a magnetic particle or a magnet, for the result of simulations as shown in Fig. 8, Fig. 9, and Fig. 10. The simulation parameters are as follows; The coils are energized with 1 amp DC current, the magnet is 12 mm in diameter and 1 mm thick and made of N35 material. The magnet moves on the coil above 1mm on the vertical axis and ∓ 18 on the horizontal axis. Thus, at any point in the 22 mm direction, it is determined how much magnetic force is applied to the magnet. The reason why the magnet was chosen as 12 mm can be explained as follows. When two coils are positioned side by side (a and b), the distance between their centers is, on average, 12 mm, although the coils differ in their designs. This measure tells us that when a coil is energized, the magnet affected by the magnetic field will be attracted toward the center (if the poles are polarized) and will reach an equilibrium point at the center. If the magnet is to be moved from coil a to coil b and the magnet diameter is smaller than the coil diameter, it cannot be moved as it will be out of the effective magnetic field, as seen in the magnetic field graphs. That's why the magnet diameter is taken to be approximately equal to the coil diameters.

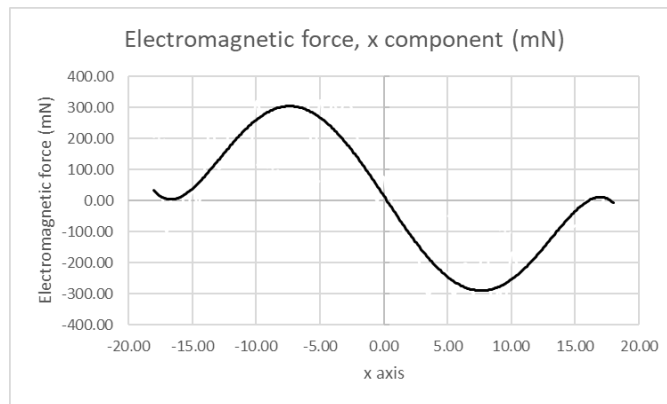


Fig. 8. Magnetic force on a 12×1 mm circular N35 magnet of circular coil

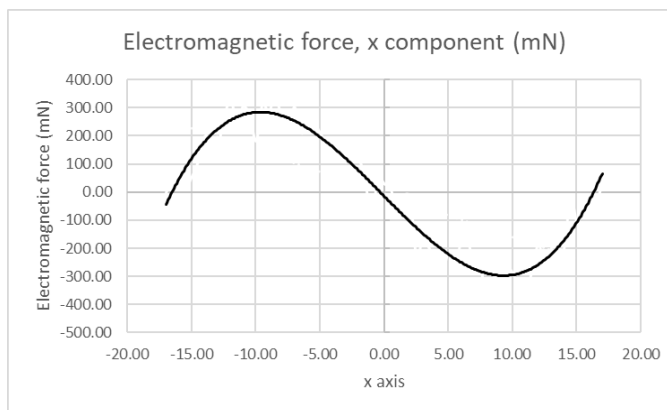


Fig. 9. Magnetic force on a 12×1 mm circular N35 magnet of square coil

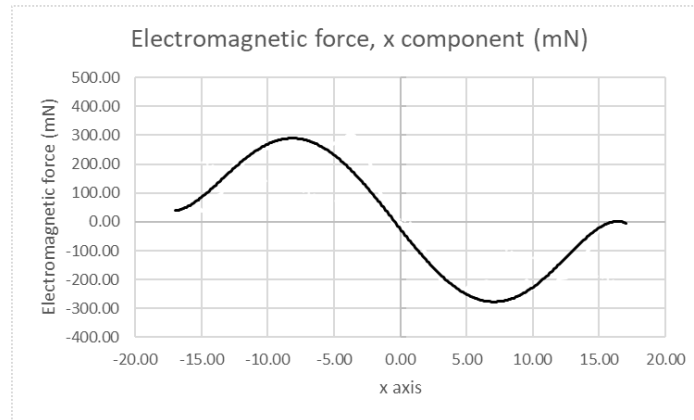


Fig. 10. Magnetic force on a 12×1 mm circular N35 magnet of hexagonal coil

3.4. Frequency Response and Characteristic Impedance

Frequency Response describes the range of frequencies that how an individual electronic system responds to the applied frequency. Since coils are part of the system, the term frequency response is inadequate for it, so in order to express impedance accurately, the term needs to be added. Fig. 11 shows impedance graphs of circular coil. In 1 Hz to 5 kHz region, coil behaves as resistor. In 5 kHz to 20 MHz region, impedance rises dramatically. In this region, inductance is dominant; beyond 20 Mhz, parasitic capacitance is dominant, so impedance is decreasing. In order to pass enough current to activate the electromagnet, the working frequency should be below 50 kHz. Because all coils perform similarly, only circular coil simulation data is shared.

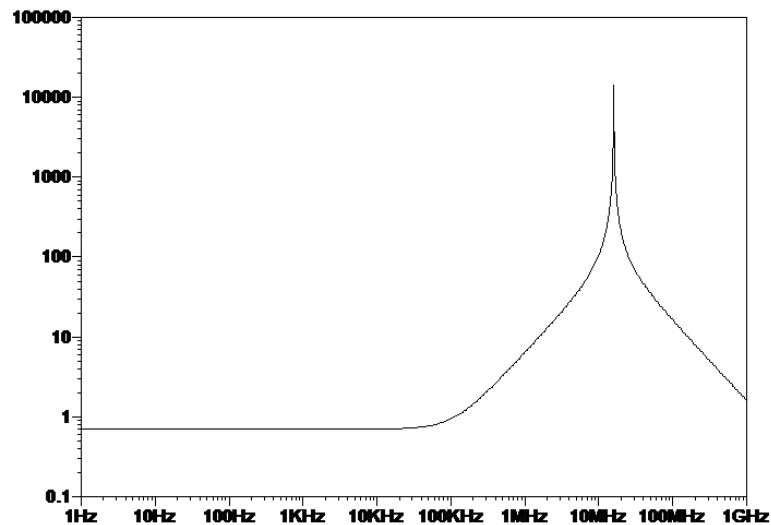


Fig. 11. Impedance graph of circular coil

3.5. Discussion

As shown in the results, calculation overlaps with calculated values. There is a 5~10% difference because of measurement tools that we are using. For the comparison of the coil that we are examining, it is necessary to look at several distinctive features and choose the best among them. It is necessary to determine the application environment well. Comparison parameters can be listed as follows;

3.5.1. Coil Shape and Layout

Since all of the coils that are simulated and tested perform similarly, another best way to compare PCB coils is their layout on the PCB and trace routing. This means how much space the intended coil occupy when used in the design and how efficiently it can use this space. As a result, the more efficiently a coil can use the area, the smaller the design size can be and the easier it will

be to move the ferromagnetic particle or magnet that moved on it, increasing the system efficiency. Another important aspect is how easily the electrical connections of the coils can be connected to a connector and power element. As a result, these coils should be energized in some way, and this electrical connection should be as short as possible (to avoid creating parasitic resistance and inductance) and not have a disruptive effect on the magnetic field.

3.5.2. Magnetic Field Magnitude and Distribution

Although the magnetic field produced by PCB coils varies according to the number of turns, diameters (widths), current and winding structures, it is very difficult to make a calculation that predicts the magnetic field strength and magnetic field distribution. Therefore, they should be analyzed with programs that simulate finite elements. As seen in Fig. 8, Fig. 9 and Fig. 10, a series of analyses were made to understand the magnetic field and distributions of the coils. In the graphs obtained, the center of the coil is at the zero point, and the distribution is analyzed in positive and negative directions on an axis. In order to compare the coils, the peak and average magnetic field strength and magnetic field distribution are examined. Thus, it can be predicted how much attraction or repulsion force will be at which distance between the ferromagnetic particle or the permanent magnet and the coil.

3.5.3. Magnetic Force

Because the tested PCB coils with very few turns and can operate relatively low currents, they produce a smaller magnetic field than conventional electromagnets on the market. And also, since they do not have a magnetic core, the magnetic field they create has a bell-shaped structure. The proposed and tested application is to move the permanent magnets on a 2D surface with the help of these coils. The point to be considered in such applications is that the friction force should be smaller than the pulling force. The direction of the force applied by the PCB coils to the magnet passes from the horizontal axis to the vertical axis as it approaches the center. Due to this structure of electromagnets, the friction force increases as the magnet gets closer to the center.

4. Conclusion

As expected, PCB coils create a magnetic field like small electromagnets, and with the magnetic field they produce, they can create a pulling force of 300~350 mN on a 12×1 mm Neodymium magnet 1mm above the PCB coil center and attract the magnet 5-6 mm away from the center of PCB coil. The fact that pulling force gradually decreases with distance as the magnet gets away from the PCB coil, at which point the coil is no longer able to attract the magnet due to friction force. That means in order to enlarge a suitable working area, friction force between that one face of the magnet and the surface of the bed needs to be precisely controlled. Also, friction force can be compensated by increasing pulling force created by PCB coil with increasing operating current, but this situation in itself causes new problems. Coils can overheat, and to prevent this situation, heatsinks that are thin enough to fit between the coil and the magnet should be placed. If we compare geometry-wise, approximately 5% magnetic field strength difference, therefore, magnetic force difference is observed between coil types. Accordingly, it would be more reasonable to use the coil type that uses the area most efficiently. These reasons are to put the square coil ahead of the others. The square coil features the highest surface area compared to other coil types with the same design parameters. When two square coils are placed on the PCB, there is no space between them except for the gap to provide electrical isolation and also for being used in possible actuators that are geometrically most suitable for the Cartesian motion system.

Even the magnetic field produced by PCB coils and, therefore, the magnetic repulsion and pull force they can create is low, they are promising enough to be used in some niche jobs that need specific working nature of PCB coils, for example, working areas that have small available space to put actuator or very strict demands on contactless handling. In future studies, a coil type will be selected by optimizing between coils that provide magnetic field generation and ease of layout, and it is planned to make a planar actuator with this coil. This planar PCB action is planned to be in the form of a 5x5 matrix consisting of the selected coil type. It is envisaged that by manipulating a permanent magnet with a planar actuator and using this permanent magnet's stronger magnetic field, it can

precisely move ferromagnetic particles. In addition, by using the advantage of being PCB coils, it is aimed to integrate the driver and controller circuits into the actuator and achieve a more compact or modular structure.

Author Contribution: All authors contributed equally to the main contributor to this paper. All authors read and approved the final paper.

Funding: This research was funded by İzmir Kâtip Çelebi University with grant number 2022-TYL-FEBE-0007.

Acknowledgment: Authors would like to acknowledge Dr. Serkan Doğanay, Dr. Nail Akçura, Gökmen Atakan Türkmen for their valuable comments.

Conflicts of Interest: The authors declare no conflict of interest.

References

- [1] W. Wang and C. Zhou, "A Journey of Nanomotors for Targeted Cancer Therapy: Principles, Challenges, and a Critical Review of the State-of-the-Art," *Advanced Healthcare Materials*, vol. 10, no. 2, 2021, <https://doi.org/10.1002/adhm.202001236>.
- [2] M. Zhang, L. Yang, C. Zhang, Z. Yang, and L. Zhang, "A 5-D Large-Workspace Magnetic Localization and Actuation System Based on an Eye-in-Hand Magnetic Sensor Array and Mobile Coils," in *IEEE Transactions on Instrumentation and Measurement*, vol. 72, pp. 1-11, 2023, <https://doi.org/10.1109/TIM.2023.3238693>.
- [3] B. Ahmad, M. Gauthier, G. J. Laurent, and A. Bolepion, "Mobile Microrobots for In Vitro Biomedical Applications: A Survey," in *IEEE Transactions on Robotics*, vol. 38, no. 1, pp. 646-663, Feb. 2022, <https://doi.org/10.1109/TRO.2021.3085245>.
- [4] S. -C. Yao *et al.*, "Micro-electro-mechanical systems (MEMS)-based micro-scale direct methanol fuel cell development," *Energy*, vol. 31, no. 5, pp. 636-649, April 2006, <https://doi.org/10.1016/j.energy.2005.10.016>.
- [5] B. Ahmad, A. Barbot, G. Ulliac, and A. Bolepion, "Hybrid Optothermal-Magnetic Mobile Microgripper for In-Liquid Micromanipulation," in *IEEE Robotics and Automation Letters*, vol. 8, no. 3, pp. 1675-1682, March 2023, <https://doi.org/10.1109/LRA.2023.3242168>.
- [6] D. Rivas, S. Mallick, M. Sokolich, and S. Das, "Cellular Manipulation Using Rolling Microrobots," *2022 International Conference on Manipulation, Automation and Robotics at Small Scales (MARSS)*, pp. 1-6, 2022, <https://doi.org/10.1109/MARSS55884.2022.9870486>.
- [7] WW. Jung, S. Lee, J. Lee, and Y. Hwang, "Wirelessly Powered Micro Soft Bellows Actuator with 3D Helix Coils," *2022 IEEE 35th International Conference on Micro Electro Mechanical Systems Conference (MEMS)*, pp. 361-364, 2022, <https://doi.org/10.1109/MEMS51670.2022.9699778>.
- [8] H. Lu, Y. Liu, Y. Yang, X. Yang, R. Tan, and Y. Shen, "Self-Assembly Magnetic Chain Unit for Bulk Biomaterial Actuation," in *IEEE Robotics and Automation Letters*, vol. 4, no. 2, pp. 262-268, April 2019, <https://doi.org/10.1109/LRA.2018.2887205>.
- [9] M. Meng, A. Ibrahim, and M. Kiani, "Design considerations for ultrasonic power transmission to millimeter-sized implantable microelectronics devices," *2015 IEEE Biomedical Circuits and Systems Conference (BioCAS)*, pp. 1-4, 2015, <https://doi.org/10.1109/BioCAS.2015.7348295>.
- [10] H. -S. Lee, E. Choi, B. Kang, J. -O. Park, and C. -S. Kim, "Gravity Directional Position Control of a Micro-particle through Frequency Variation of a Single Ultrasonic Transducer," *2019 12th Asian Control Conference (ASCC)*, pp. 353-357, 2019, <https://ieeexplore.ieee.org/abstract/document/8765014>.
- [11] F. X. Hart, "Integrins May Serve as Mechanical Transducers for Low-Frequency Electric Fields," *Bioelectromagnetics*, vol. 27, no. 6, pp. 505-508, 2006, <https://doi.org/10.1002/bem.20236>.
- [12] X. Lu, Y. Yan, B. Qi, H. Qian, J. Sun, and A. Quigley, "Contactless Haptic Display Through Magnetic Field Control," in *IEEE Transactions on Haptics*, vol. 15, no. 2, pp. 328-338, 2022, <https://doi.org/10.1109/TOH.2022.3151673>.

-
- [13] C. Yu *et al.*, “Novel electromagnetic actuation system for three-dimensional locomotion and drilling of intravascular microrobot,” *Sensors and Actuators A: Physical*, vol. 161 issues 1–2, pp. 297-304, 2010, <https://doi.org/10.1016/j.sna.2010.04.037>.
- [14] X. Fan, X. Dong, A. C. Karacakol, H. Xie, and M. Sitti, “Reconfigurable multifunctional ferrofluid droplet robots,” *Proceedings of the National Academy of Sciences of the United States of America*, vol. 117, no. 45, pp. 27916-27926, 2020, <https://doi.org/10.1073/pnas.2016388117>.
- [15] C. R. Thornley, L. N. Pham, and J. J. Abbott, “Reconsidering Six-Degree-of-Freedom Magnetic Actuation Across Scales,” in *IEEE Robotics and Automation Letters*, vol. 4, no. 3, pp. 2325-2332, July 2019, <https://doi.org/10.1109/LRA.2019.2902742>.
- [16] P. Punyabrahma, G. R. Jayanth, and A. K. Mohanty, “Trapping and 3-D Manipulation of Magnetic Microparticles Using Parametric Excitation,” in *IEEE Robotics and Automation Letters*, vol. 7, no. 2, pp. 1403-1407, April 2022, <https://doi.org/10.1109/LRA.2021.3138164>.
- [17] M. C. Hoang *et al.*, “Independent Electromagnetic Field Control for Practical Approach to Actively Locomotive Wireless Capsule Endoscope,” in *IEEE Transactions on Systems, Man, and Cybernetics: Systems*, vol. 51, no. 5, pp. 3040-3052, May 2021, <https://doi.org/10.1109/TSMC.2019.2917298>.
- [18] J. Sikorski, C. M. Heunis, F. Franco, and S. Misra, “The ARMM System: An Optimized Mobile Electromagnetic Coil for Non-Linear Actuation of Flexible Surgical Instruments,” in *IEEE Transactions on Magnetics*, vol. 55, no. 9, pp. 1-9, Sept. 2019, <https://doi.org/10.1109/TMAG.2019.2917370>.
- [19] G. A. Türkmen, S. Doğanay, L. Çetin, and A. Turgut, “Ferrofluid Droplet Robot Manipulation Using Rule-Based Control Strategy,” *2022 IEEE XVIII International Conference on the Perspective Technologies and Methods in MEMS Design (MEMSTECH)*, pp. 16-19, 2022, <https://doi.org/10.1109/MEMSTECH55132.2022.10002916>.
- [20] D. J. Cappelleri, J. Fink, B. Mukundakrishnan, V. Kumar, and J. C. Trinkle, “Designing open-loop plans for planar micro-manipulation,” *Proceedings 2006 IEEE International Conference on Robotics and Automation, 2006. ICRA 2006.*, pp. 637-642, 2006, <https://doi.org/10.1109/ROBOT.2006.1641782>.
- [21] Y. Shi, Z. Xin, P. C. Loh, and F. Blaabjerg, “A Review of Traditional Helical to Recent Miniaturized Printed Circuit Board Rogowski Coils for Power-Electronic Applications,” in *IEEE Transactions on Power Electronics*, vol. 35, no. 11, pp. 12207-12222, Nov. 2020, <https://doi.org/10.1109/TPEL.2020.2984055>.
- [22] D. Suwandi, R. Aziz, A. Sifa, E. Haris, J. Istiyanto, and Y. Whulanza, “Dry Film Photoresist Application to a Printed Circuit Board (PCB) Using a Maskless Photolithography Method,” *International Journal of Technology*, vol. 10, no. 5, pp. 1033-1041, 2019, <https://doi.org/10.31224/osf.io/27f49>.
- [23] H. Rao C., B. K. S. V. L. Varaprasad, and S. Goel, “Direct Ink Writing as an Eco-Friendly PCB Manufacturing Technique for Rapid Prototyping,” *2021 Fourth International Conference on Electrical, Computer and Communication Technologies (ICECCT)*, pp. 1-7, 2021, <https://doi.org/10.1109/ICECCT52121.2021.9616903>.
- [24] Y. Liu, X. Xie, Y. Hu, Y. Qian, G. Sheng, and X. Jiang, “A Novel Transient Fault Current Sensor Based on the PCB Rogowski Coil for Overhead Transmission Lines,” *Sensors*, vol. 16, no. 5, pp. 742, 2016, <https://doi.org/10.3390/s16050742>.
- [25] R. Zhang, D. Zhang, and R. Dutta, “Study on PCB Based Litz Wire Applications for Air-Core Inductor and Planar Transformer,” *2019 9th International Conference on Power and Energy Systems (ICPES)*, pp. 1-6, 2019, <https://doi.org/10.1109/ICPES47639.2019.9105549>.
- [26] N. Ebrahimi, P. Schimpf, and A. Jafari, “Design optimization of a solenoid-based electromagnetic soft actuator with permanent magnet core,” *Sensors and Actuators A: Physical*, vol. 284, pp. 276-285, 2018, <https://doi.org/10.1016/j.sna.2018.10.026>.
- [27] M. Aldoumani, B. Yuce, and D. Zhu, “Using the Variable Geometry in a Planar Inductor for an Optimised Performance,” *Electronics*, vol. 10, no. 6, p. 721, 2021, <https://doi.org/10.3390/electronics10060721>.
- [28] NFC/RFID Planar Spiral Coil Inductance Calculator. <https://www.translatorscafe.com/unit-converter/en-US/calculator/planar-coil-inductance/>
-

- [29] S. S. Mohan, M. del Mar Hershenson, S. P. Boyd, and T. H. Lee, "Simple accurate expressions for planar spiral inductances," in *IEEE Journal of Solid-State Circuits*, vol. 34, no. 10, pp. 1419-1424, Oct. 1999, <https://doi.org/10.1109/4.792620>.
- [30] IPC, IPC-2221A: Generic standard on printed board design, IPC, 1998, [http://www-eng.lbl.gov/~shuman/NEXT/CURRENT_DESIGN/TP/MATERIALS/IPC-2221A\(L\).pdf](http://www-eng.lbl.gov/~shuman/NEXT/CURRENT_DESIGN/TP/MATERIALS/IPC-2221A(L).pdf)
- [31] A. Bhattacharjee, L. W. Rogowski, X. Zhang, and M. J. Kim, "Untethered Soft Millirobot with Magnetic Actuation," *2020 IEEE International Conference on Robotics and Automation (ICRA)*, pp. 3792-3798, 2020, <https://doi.org/10.1109/ICRA40945.2020.9197202>.